Combining the All-Source Green's Functions and the GPS-Derived Source Functions for Fast Tsunami Predictions—Illustrated by the March 2011 Japan Tsunami

ZHIGANG XU

Maurice Lamontagne Institute, Fisheries and Oceans Canada, Mont-Joli, Quebec, Canada

Y. TONY SONG

Jet Propulsion Laboratory, California Institute of Technology, Pasadena, California

(Manuscript received 19 September 2012, in final form 12 January 2013)

ABSTRACT

This paper proposes an effective approach on how to predict tsunamis rapidly following a submarine earthquake by combining a real-time GPS-derived tsunami source function with a set of precalculated all-source Green's functions (ASGFs). The approach uses the data from both teleseismic and coastal GPS networks to constrain a tsunami source function consisting of both sea surface elevation and horizontal velocity field, and uses the ASGFs to instantaneously transfer the source function to the arrival time series at the destination points. The ASGF can take a tsunami source of arbitrary geographic origin and resolve it as fine as the native resolution of a tsunami propagation model from which the ASGF is derived. This new approach is verified by the 2011 Tohoku tsunami using data measured by the Deep-Ocean Assessment and Reporting of Tsunamis (DART) buoys.

1. Introduction

The Green's functions to the linear shallow-water dynamics system play an indispensable role in tsunami research and real-time warnings. Their earlier applications were mostly for postevent inversion problems to infer about tsunamis' sources or fault displacements given the observed tsunami waves (e.g., Satake 1985, 1987, 1989; Johnson and Satake 1993, 1996). While this stream of efforts still continues (e.g., Fujii and Satake 2007, 2008; Fujii et al. 2011; Romano et al. 2012), their applications have been recently pushed into real-time tsunami forecasts (e.g., Titov et al. 2005; Lauterjung and the GITEWS Team 2008). Because the Green's functions can be precalculated and a tsunami source can be estimated based on seismic information (such as epicenter and magnitude) in real time, it is possible to quickly and still fairly accurately calculate the amplitudes and arrival times of tsunami waves at a destination point of interest (POI).

When a dynamic system is not simple, as is the case for a real ocean, its Green's function has to be obtained numerically by running a numerical model, which discretizes the shallow-water equations in our case, with a model grid point taken as the source point for an impulsive force. A Green's function so obtained is only valid for that source point, and we call it a single-source Green's function (SSGF) in this paper. Merely one SSGF is not useful, since a future tsunami may not be sourced just at the prespecified point, and even if it is so, it will unlikely only occupy a single grid cell. Hence, a concept of source zone has come into practice. A source zone is a geographic region, consisting of a set of grid points that can all be the source points potentially. For earthquake-generated tsunamis, the source zone may be assumed along boundaries of some tectonic plates. This cuts the distribution of potential source points greatly from otherwise in the whole domain (such as for the storm surge problems) to a (or a few) narrow zone(s). Ideally, if computational workload and data storage are not a problem, then one should take each grid point in turn in the source zone as the unit source and repeat the model runs to compute a set of Green's functions. This way, a future tsunami could be allowed to be sourced anywhere in the zone and whose spatial distribution

Corresponding author address: Zhigang Xu, Maurice Lamontagne Institute, Fisheries and Oceans Canada, 850, Route de la Mer, P.O. Box 1000, Mont-Joli QC G5H 3Z4, Canada.
E-mail: zhigang.xu@dfo-mpo.gc.ca

DOI: 10.1175/JTECH-D-12-00201.1

could be resolved in the tsunami propagation model's native resolution.[1] However, although the source area has been restricted to a narrow zone, a narrow zone can still be very long (such as the Pacific Ring of Fire), and there are still too many grid points to be treated as source points individually. To reduce the computational workload and the data storage, a block–source concept has thus come into practice: many grid points are lumped into one block on which a unit source is placed collectively. We call a Green's function so obtained a block–source Green's function (BSGF) hereafter.

The National Oceanic and Atmospheric Administration (NOAA) Center for Tsunami Research (NCTR) has been developing a tsunami forecasting system, called Short-Term Inundation Forecasting for Tsunamis (SIFT), intended for operational use by NOAA (Gica et al. 2008; also see NCTR 2012b,d). The SIFT system assumes the entire Pacific Ring of Fire and parts of coastal margins of the Indian and Atlantic Oceans as tsunami source zones and uses blocks of 100 km × 50 km to tile the zones. A key component of the system is a tsunami propagation database, composed of a set of precalculated unit–source-driven tsunami solutions, which can be pulled out quickly in real time to form linear combinations as the responses in water levels at some POIs to an arbitrary tsunami source. The SIFT system has so far built up nearly 1700 BSGFs, whose source blocks were selected from different sectors of the source zones (NCTR 2012e), presumably according to a priority order. With data assimilation, good agreements between the linear combinations and the observations by the Deep-Ocean Assessment and Reporting of Tsunamis (DART) buoys (NCTR 2012a) were reported for the 2011 Japan tsunami (NCTR 2012c).

Strictly speaking, a Green's function is defined only for a liner system. We noticed, however, that a nonliner model, called the Method of Splitting Tsunami (MOST) model (Titov and González 1997), was used by the SIFT system to produce the unit–source solutions. However, the fact that the linear combinations of those unit–source solutions agree well with the observations implies that the nonlinear components in the unit–source solutions are not important, at least for the places where DART buoys are. Otherwise, the linear superposition principle would be severely violated and we would not see the good agreements. This also agrees with what Shuto (1991, p. 181) said: ''In seas deeper than 50 m the linear long wave theory gives satisfactory results.'' Therefore, the unit–source solutions in the SIFT system may well be regarded as Green's functions. In fact, in some SIFT-related publications, the Green's functions and the propagation database are used interchangeably (e.g., Titov et al. 2005; Weinstein and Lundgren 2008). Using a nonlinear model to generate Green's functions for linear superposition is also reported in Romano et al. (2012).

The Green's function approach is also adopted by another tsunami warning system, the German–Indonesian Tsunami Early-Warning System (GITEWS; Lauterjung and the GITEWS Team 2008). The GITEWS regards the Sunda (Java) Trench to be the potential tsunami source zone, using blocks of 45 km × 15 km to cover the zone. Therefore, a preassumed source zone plus a set of blocks tiling the source zone has been a common approach to prepare the Green's functions. However, the location of the source zone and the sizes of the blocks limit the usefulness of the prepared Green's functions. If a future tsunami is triggered outside of the preassumed source zone, then the prepared Green's function will not be useful. Also, the block sizes limit the resolution of a source function that can be used. Since the block sizes are much larger than the grid spacing (otherwise there is no need to introduce blocks), a source function could not be resolved as fine as the native resolution of a tsunami propagation model.

It may be debatable how severe these restrictions are; however, we actually do not have to bear them at all. Xu (2007, 2011) presented a new type of Green's function, called the all-source Green's function (ASGF). In contrast to an SSGF, which focuses on a source point, an ASGF focuses on a receiver point, regarding *all* the model grid points as potential source points. An ASGF may be interpreted as a dependence field of the wave solution (at the receiver point) on the initial conditions everywhere (in terms of both elevations and velocities, and distributed possibly anywhere in the entire computational domain). The calculation for an ASGF starts from a receiver point and builds up outward the dependence field. The domain of the dependence field grows with time. A 24-h dependence field can sufficiently cover the entire Pacific Ocean (see section 2 for more details). This receiver-focus approach is a much safer approach than the traditional source-focus approach. It is not certain where the next tsunami will be sourced but everyone knows where their points of interest are. The features of an ASGF may be summarized as follows: 1) it covers sources of arbitrary geographic origins and spatial distributions, and the source coverage is global; 2) it allows sources to be resolved in the tsunami model's *native resolution*; 3) it supports *both elevation and velocity components* in source functions, and inclusion of the velocity components comes at no

[1] By the native resolution, we mean the grid spacing of a tsunami propagation model with which the Green's functions are calculated.

additional computational cost; and 4) the number of ASGFs to be precalculated is the number of the POIs that we may desire; if we have only one POI, then we will have one ASGF to prepare.

To forecast tsunamis in real time, another critical issue is how to obtain a reliable tsunami source as soon as a tsunami-triggering event occurs. For earthquake-generated tsunamis, slip models, such as Okada (1985), based on initial earthquake parameters (e.g., epicenter, fault size, rake angle, and magnitude) have been the primary means to obtain a source. Such a magnitude-based estimate can offer a quick input to start off the forecast system, but it is only a preliminary estimate and yet to be refined. The SIFT system performs the refinements with inversions of the data stream from DART buoys when tsunami waves arrive there. To wait for tsunami waves to reach the observation sites consumes precious time, however.

Song (2007) and Song et al. (2008) proposed an alternative method of using real-time GPS data from a coastal GPS-station network that measures the earthquake-induced ground motions (called the GPS method). Based on the impulse–momentum theory (Song et al. 2008), the GPS data are used to convert the impulses of the continental slope to the initial momentum of the surrounding water columns. Complemented with seismic waveform inversion (Song et al. 2005; Song and Han 2011), a tsunami source function that contains both the initial sea levels and initial water velocities components can be made available in a matter of a few minutes (called the GPS-derived source). The March 2011 Japan earthquake provides an excellent case to test their theory. About 1200 GPS stations with an average spacing of 20 km over Japan provided probably the most complete, prompt, and densest measurement of near-field ground motions ever for an earthquake with such a magnitude.

So far the Green's functions seen in the publications were obtained with unit sources of sea levels only. In reality, it is possible to have nonzero initial velocities because of the horizontal impacts of continental slopes (Song et al. 2008). However, it seems that, so far, they have been neglected. This is perhaps partially because it is hard to estimate the initial velocities, and partially because adding the two velocity components would triple the workload for preparing the Green's functions with the traditional approach.

Although the ASGF method and the GPS method have both been published independently, how the two methods can work together for a real tsunami case has not been explored yet. In this paper we will report on our exploration with the 2011 Japan tsunami as the test case. This real tsunami case is an excellent case, for which there are abundant observations of both coastal-based GPS data and the deep-ocean DART buoys data. We hope that our exploration will bring forward an alternative or parallel approach for establishing a tsunami-predicting system. Real-time tsunami prediction is an important and challenging subject, requiring constant efforts to improve or enrich its methodology.

In section 2, we will describe the model domain, the governing equations, and the ASGFs for the tsunami wave propagations. Section 3 will describe the GPS-derived source function for the 2011 Tohoku tsunami. In section 4 we will test the performances of the GPS-derived source and the ASGFs against the DART buoy data. Section 5 will give a summary and discussions of our results. We will also include two appendixes. Appendix A will give an algorithm on how to calculate the ASGF. Appendix B will outline how the source function is calculated from the coastal-based GPS data.

2. Model domain, governing equations, and ASGFs for tsunami waves

This section describes the model domain, and the governing equations for tsunami wave propagation in both continuous and discretized forms, and interprets the physical meaning of ASGFs.

a. Model domain and grid

The model domain is shown in Fig. 1. The domain covers the Pacific, the Indian, and the Southern Oceans. The grid spacing is 5 min in both longitude and latitude (which is what we have referred to as the native resolution of the tsunami propagation model). The topography used in the model is decimated from a 30-s global topography database, the General Bathymetric Chart of the Oceans (GEBCO08; http://www.gebco.net). The model variables are arranged according to the Arakawa C grid (Arakawa and Lamb 1977). The maximum water depth is 10 545 m, and the minimum water depth is set to be 10 m. The maximum time step constrained by the Courant–Friedrichs–Lewy (CFL) condition is 5.3610 s but rounded to 5 s for convenience in managing the model outputs. There are ~~more than~~ 11 338 490 grid points on which model variables are defined.

b. Governing equations for tsunami wave propagations

As mentioned in the introduction, propagation of tsunami waves in deep water (>50 m) well obey linear dynamics. Hence, we choose the linear shallow-water equations to govern the tsunami propagations. The equations can be expressed in matrix form as

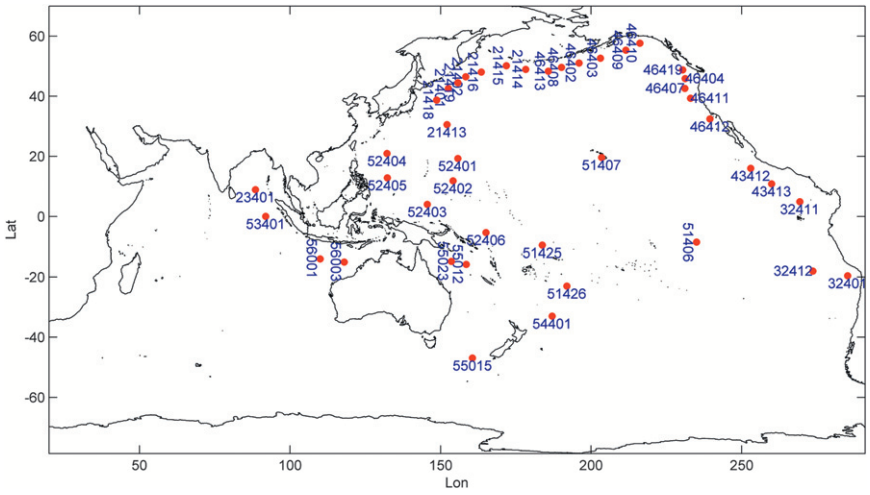

FIG. 1. Model domain covering the Pacific, Indian, and Southern Oceans. DART stations as identified by the red dots and their station numbers are taken as POIs in this paper.

$$\frac{\partial}{\partial t}\begin{bmatrix}\eta\\ U\\ V\end{bmatrix} = -\begin{bmatrix} 0 & \dfrac{\partial}{\partial x} & \dfrac{\partial \cos\phi}{\cos\phi\,\partial y}\\ gh\dfrac{\partial}{\partial x} & \dfrac{\kappa}{h} & -f\\ gh\dfrac{\partial}{\partial y} & f & \dfrac{\kappa}{h}\end{bmatrix}\begin{bmatrix}\eta\\ U\\ V\end{bmatrix}. \qquad (1)$$

In the above equation, t is the time variable, and x and y are the arc lengths along circles of latitude and longitude, respectively, and are related to the longitude λ, latitude φ, and Earth's mean radius R (taken as the volumetric radius = 6371 km; Moritz 2000) by $x = R\lambda\cos\phi$, and $y = R\phi$; $(\partial/\partial x) \equiv (\partial/R\cos\phi\partial\lambda)$ and $(\partial/\partial y) \equiv (\partial/R\partial\phi)$; η, U and V are the sea surface elevation, and the mass fluxes in longitudinal and latitudinal directions; f and g are the Coriolis parameter and gravity acceleration; h and κ are the water depth and bottom frictional coefficient, respectively. Note that the partial derivative operator in the matrix affects all the factors that come to its right side, for example, the multiplication of $\partial\cos\phi/\cos\phi\partial y$ with V should be understood as $\partial(V\cos\phi)/\cos\phi\partial y$. Generally, there is less bottom friction in deep water than in shallow water. To reflect this fact, we follow Ding et al. (2004) and Xu (2011) (also see Tan 1992) to let the frictional coefficient be inversely proportional to the cubic root of water depth, resulting in κ ranging from 4.5×10^{-4} to $4.6\times10^{-3}\,\mathrm{m\,s^{-1}}$ in our model domain.

The boundary conditions consist of zero flows normal to the coasts,

$$U = 0 \quad \text{at the west and east coasts}, \qquad (2)$$

$$V = 0 \quad \text{at the south and north coasts}, \qquad (3)$$

and the Sommerfeld (1949) radiation conditions at open water boundaries,

$$\frac{\partial p}{\partial t} + c\frac{\partial p}{\partial n} = 0 \quad \text{at open water boundaries}, \qquad (4)$$

where p may stand for U, V, or η; c is a phase speed; and ∂n means an infinitesimal line segment along the directions outward normal to the open boundaries. For this study c is set to the long gravity wave speed, $c = \sqrt{gh}$.

In addition to the radiation boundary condition, we also place narrow "sponge zones" immediately next to open water boundaries, to largely absorb wave reflections from the artificial water boundaries. The sponge-absorbing effects are achieved by assigning larger-than-normal frictional parameter values in the zone. More details on this are described by Xu (2011).

Equations (1)–(4) define the linear dynamics system governing tsunami wave propagations. To integrate the system numerically, the equations have to be discretized both in space and in time. There are many ways for the discretization and Xu (2011) has provided one in detail. No matter what discretizing scheme one may prefer, one can always arrive at the following canonical form as the discretized version of the system:

$$\begin{bmatrix}\boldsymbol{\eta}\\ \mathbf{U}\\ \mathbf{V}\end{bmatrix}^{(k+1)} = \mathbf{A}\begin{bmatrix}\boldsymbol{\eta}\\ \mathbf{U}\\ \mathbf{V}\end{bmatrix}^{(k)}, \qquad (5)$$

where superscript k outside of the square brackets is an index for the time stepping. The coefficient matrix $\mathbf{A}$ encapsulates the model's governing equations, the boundary

conditions, and the topography. Hence, it may be referred to as the dynamic matrix. Also because it advances the state variables, $[\boldsymbol{\eta}\,\mathbf{U}\,\mathbf{V}]^{\mathrm{T}}$, from the current time step to the next, it is also referred to as the updating matrix. In computational fluid dynamics, it is known as the amplification matrix.

c. The ASGF

Let us first note that Eq. (5) can be equivalently expressed as

$$\begin{bmatrix}\boldsymbol{\eta}\\ \mathbf{U}\\ \mathbf{V}\end{bmatrix}^{(k)} = \mathbf{A}^k \begin{bmatrix}\boldsymbol{\eta}\\ \mathbf{U}\\ \mathbf{V}\end{bmatrix}^{(0)}, \quad k = 1,2,3,\ldots,k_{\max}, \tag{6}$$

where $\mathbf{A}^k$ represent the kth power of the matrix $\mathbf{A}$. In this paper, a superscripted number with parentheses indicates the time step, whereas the one without parentheses indicates an exponent. Although Eqs. (5) and (6) are mathematically equivalent, they differ dramatically in their computational costs. If the solutions at all model grid points are required, then Eq. (5) should be the choice for computational efficiency, since at each time step it only involves a matrix–vector multiplication. In this case, the choice of Eq. (6) would be unwise, since for $k \geq 2$ all the powers of the matrix $\mathbf{A}$ up to the power k would need to be calculated. This would be very expensive or infeasible when the size of the matrix is large. However, if we are only interested in the solutions at a few model grid points as is the case in reality, then Eq. (6) provides a distinct advantage as we shall demonstrate now.

Assume that there is only one POI, say the nth grid point, where the sea surface elevation is interested. According to Eq. (6) the time series of the elevation at the nth grid point can be written as

$$\boldsymbol{\eta}_n^{(k)} = \mathbf{A}^k(n,:) \begin{bmatrix}\boldsymbol{\eta}\\ \mathbf{U}\\ \mathbf{V}\end{bmatrix}^{(0)}. \tag{7}$$

The crux here is how to compute the matrix power $\mathbf{A}^k(n,:)$ economically. If we had to calculate the power of the whole matrix before we could extract the nth row from the power, then the calculation would be too expensive. Can we calculate just for the nth row of the power? The answer is yes. The algorithm given in appendix A shows how and leads to a simple matrix equation, Eq. (A2), there, which we copy here for easy reference:

$$\boldsymbol{\eta}_n(k) = \mathbf{G} \begin{bmatrix}\boldsymbol{\eta}\\ \mathbf{U}\\ \mathbf{V}\end{bmatrix}^{(0)}, \tag{8}$$

where $\mathbf{G}$ is a matrix whose rows consist of $\mathbf{A}^k(n,:)$, $k = 0,1,2,\ldots,k_{\max}$. In the above equation, $\boldsymbol{\eta}_n(k)$ represents the time series of the elevations at the nth η node. Note that the parenthesized k here is not in a superscript position. A parenthesized k in a normal position means a vector of time indexes, $k = 1, 2, \ldots, k_{\max}$. At the end of appendix A, we have also put the three types of Green's functions—the SSGFs, the BSGFs, and the ASGFs—at the same algorithmic footing, so that their differences and relations can be clearly seen.

It is the $\mathbf{G}$ matrix that defines the ASGF. The $\mathbf{G}$ matrix has N columns, with N being the number of total grid points where η, U, or V variables are defined. A column can be viewed as an information channel. Having N channels means that signals from N different sources can be simultaneously received and stored separately by a receiver. The superposition principle will allow the N-channel signals to be linearly combined to quickly yield a full solution when a real-time event happens. If we have multiple POIs, then we can construct their ASGFs one by one: one ASGF for one receiver. Practically speaking, the number of POIs is a very small number relative to the number of model grid points. As we mentioned earlier, for the 5-min-resolution domain shown in Fig. 1, there are more than 11 million grid points with the solution variables (i.e., η, U, V), whereas the number of POIs may be on an order of 10^2–10^3 practically.

Equation (8) says that a single matrix–vector multiplication provides the time series at the POI in response to an initial setup anywhere in the model domain. A single matrix–vector multiplication can be performed in no time noticeably. The performance can go even quicker if we realize that in reality a tsunami source region will only occupy a tiny portion of the whole ocean area; we can then reduce both the size of the initial vector and the number of columns of the $\mathbf{G}$ matrix dramatically. For the 2011 Tohoku tsunami, the number of nonzero elements accounts for only 0.2% of the total elements in the initial vector. This means that 99.8% of the columns of the $\mathbf{G}$ matrix can be cut down. This also means that 99.8% of the $\mathbf{G}$ matrix stored on a disk does not need to be loaded back to the RAM in the first place.

Therefore, if the needed portion of the $\mathbf{G}$ matrix has already been loaded into the RAM, then it will take no time to multiply a tall and thin matrix with a short vector. If not, then it may take a few seconds to load it into the RAM first. With a tolerance of at most a few seconds, we can say that the transfer of a tsunami source function to tsunami arrivals at a POI can always be performed instantaneously in real time. To ensure that any needed portion of the $\mathbf{G}$ matrix can be quickly retrieved from the disk, the matrix should not be saved as a single huge file.

Instead, it should be saved as many small ones. A way to achieve this has been given in Xu (2011).

For a different initial setup, corresponding to a new tsunami, one can simply substitute a new column vector for $[\boldsymbol{\eta}^{(0)}\ \mathbf{U}^{(0)}\ \mathbf{V}^{(0)}]^{\mathrm{T}}$ without modifying the matrix $\mathbf{G}$; that is, once $\mathbf{G}$ has been calculated, it can be repeatedly used. The evolution from any specified initial state is easily calculated from a single matrix–vector multiplication. The preparation of the matrix $\mathbf{G}$ may require significant computer resources, but the matrix–vector multiplication can be quickly performed even on an ordinary personal computer or on a web server.

Note that Eq. (8) explicitly shows that both the surface elevations and the velocities (or precisely speaking, the mass fluxes per unit width) form a source function. We will demonstrate the importance of including the velocity source functions when we apply our methods to the 2011 Tohoku tsunami.

d. The field of dependence of the wave solutions

What an ASGF describes is a *field of dependence:* the dependence of wave solutions at one point on the initial conditions distributed in the model domain. Figure 2 should remind us of the classical concept of domain of dependence of the 1D wave solution: the solution at a spatial–temporal point (x, t) depends only on the initial condition distributed on the interval $[x-ct, x+ct]$, where c is the wave speed. The interval grows with time at the same rate as the wave speed c.

A wave solution at a point on the 2D Earth surface has a domain of dependence too. However, this seems to have received little attention in practice, perhaps owing to the fact that it is hard to visualize this domain from solutions obtained with a conventional modeling approach. Now with an ASGF, one can not only see the domain of dependence but also know weights of the dependence. We call the domain and weights of dependence collectively a field of dependence. Figure 3 shows the time evolution of the field of dependence of the wave solutions at a POI offshore of Hawaii (where the DART 51407 buoy is located). The boundary between the colored and noncolored regions outlines the domain of dependence, which grows with time, as illustrated by the four panels of the figure. The different colors indicate different weights of the dependence, which can be either positive or negative. A negative weight means that a positive/negative source will cause a negative/positive response at the POI. Any source function outside of the domain of dependence cannot affect the solutions at the POI at that time. The source region of the 2011 Tohoku tsunami is outlined by the red box on the bottom-right panel, indicating that nearly 8 h are needed for the tsunami to impact Hawaii.

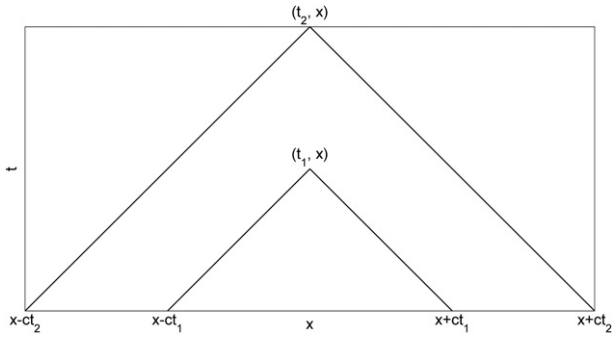

FIG. 2. Domain of dependence of a 1D wave solution. Solution at a temporal–spatial point (t, x) only depends on the initial conditions within the interval of $[x-ct\ x+ct]$. Conditions outside the interval have no effects on the solution at the time in question. Domain of the interval grows with time with a rate equal to the wave speed c.

3. The 2011 Tohoku source function

To obtain the tsunami source function from the real-time GPS data for the 2011 Tohoku tsunami, we use a three-dimensional source model that includes both the vertical displacement of seafloor, which is directly transferred to a sea surface elevation perturbation, and the impulse–momentum perturbation due to the horizontal motion of continental slopes. When a large-scale continental section slips into the ocean due to an earthquake, a transfer of momentum occurs and a three-dimensional force is exerted on the fluid. This methodology has been successfully demonstrated by Song (2007), Song and Han (2011), and Song et al. (2008, 2012). For completeness, the method is briefly summarized in appendix B. Equations (B4)–(B6) give the initial elevation field and the initial water mass transport field. The fields are defined regularly on the grid points, from which one can easily construct an initial vector $[\boldsymbol{\eta}^{(0)}\ \mathbf{U}^{(0)}\ \mathbf{V}^{(0)}]^{\mathrm{T}}$ and render it seamlessly to Eq.(8), which can then immediately transfer the initial vector to the time series of tsunami arrivals at the predetermined destination point for which the $\mathbf{G}$ matrix was prepared.

Japan has deployed an advanced near-real-time network of GPS stations that can monitor the three-dimensional ground motions across Japan. This GPS network consists of about 1200 stations with an average spacing of 20 km over Japan and comprises the largest GPS monitoring array in the world. Soon after the Tohoku earthquake, the Advanced Rapid Imaging and Analysis (ARIA) Center for Natural Hazards at the Jet Propulsion Laboratory (JPL) and the California Institute of Technology used the observations from this network to provide a solution for the coseismic displacements. The GPS data obtained during the Tohoku earthquake are probably the most complete, prompt, and densest

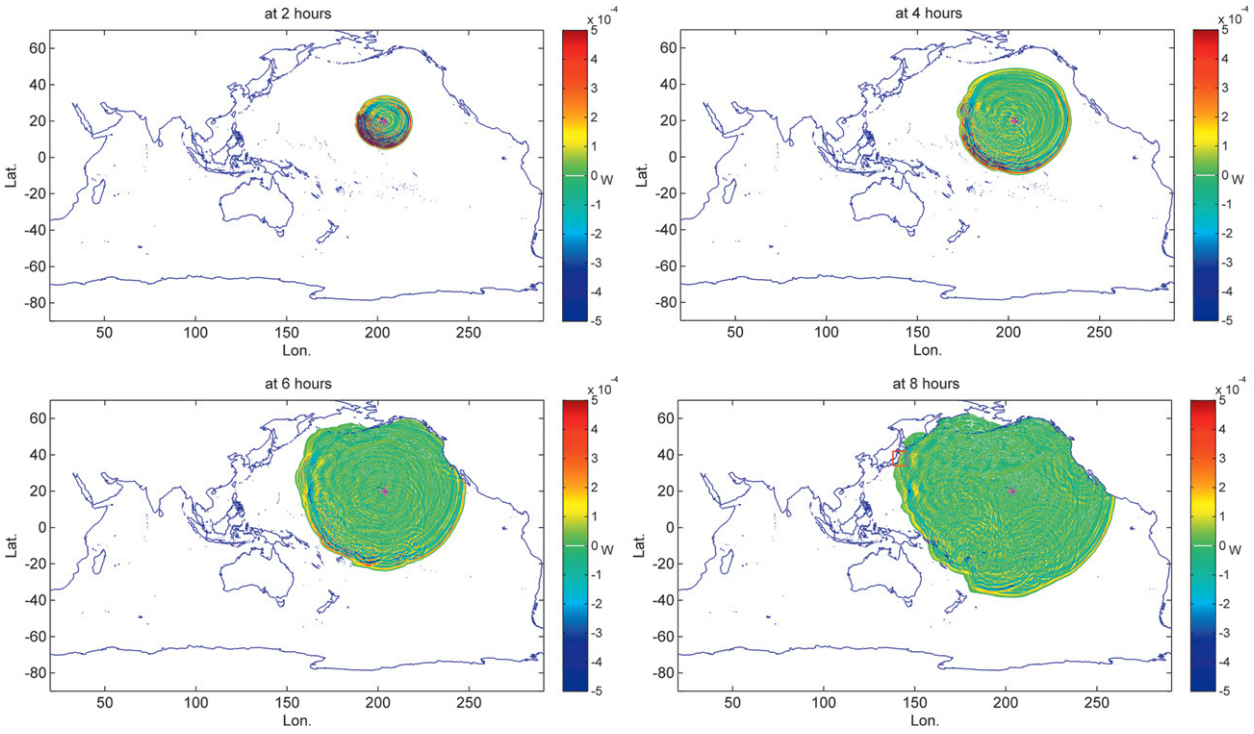

FIG. 3. Time evolution of the field of dependence of the wave solutions at a POI offshore of Hawaii (DART 51407). Boundary between the colored and noncolored regions outlines the ever-growing domain of dependence. Colors indicate the ever-changing weights of dependence. Indicated by the red box in the bottom-right panel is the source region of the 2011 Tohoku tsunami, showing that it takes about 8 h before the Tohoku tsunami can affect Hawaii.

measurement of near-field ground motions ever for an earthquake with such a magnitude.

Using the land-based GPS data and the empirical profile method of Song (2007), we estimated the tsunami source, including the horizontal displacement and vertical uplift of the seafloor that were responsible for the tsunami. The left panel of Fig. 4 gives the initial sea levels and the horizontal velocities of the initial water motion as derived from the GPS data. Similarly, the right panel of Fig. 4 shows the initial sea levels and the initial water mass transport (the depth integrated and per unit width). It is the depth-integrated water mass transports that matter in the sea levels. This figure reveals that the earthquake resulted in an initial water movement to the east, with depth-averaged velocities on order of 0.5 m s^{-1}. The largest initial sea level setup is about 9 m, peaked at the eastern boundary of the source region, followed by a broad but very shallow depression (negatively valued). The spatial resolution of the source is 5 min in both longitude and latitude.

4. The predictions and comparisons with the DART observations

With the above-mentioned tsunami initial condition, we are now ready to use Eq. (8) to predict Tohoku tsunami arrivals at POIs. We have taken the positions of the DART buoys as our validating POIs and have calculated all of their **G** matrices. The precalculated **G** matrices enable us to quickly predict time series of tsunami arrivals at these buoys upon specifying a source function for a particular event no matter how far apart the source region and the buoys are. As shown in Fig. 4, there are three components in our source function: the initial sea levels η, and the initial water mass transports **U** and **V**. Although our primary interest is to know how the total water levels driven by these three components together, it is also interesting to know their individual contributions to the observed signals. With our matrix approach, it is very easy to perform such an investigation, simply by retaining one component and zeroing out the others in the initial vector in Eq. (8).

Shown in Fig. 5 are different versions of the prediction against the same observation for station DART 21418. The prediction in the top-left panel is made with all three components of the source function. This prediction agrees well with the observation in terms of the arrival times, the largest amplitude (the primary wave), and the overall patterns of the time series. The spikes in red at the beginning of the observed curve are not water waves; they are seismic waves propagating in the lithosphere and

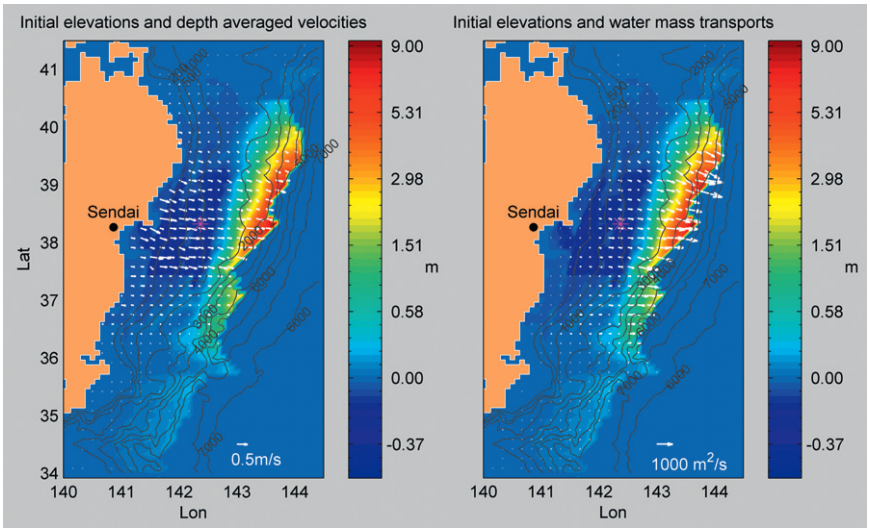

FIG. 4. Source function for the 2011 Tohoku tsunami. Colors as scaled by the color bar represent the sea surface elevations in meters and the white arrows represent the (left) depth-averaged velocities and (right) depth-integrated water mass transport (per unit width). Scale of the color bar is nonlinear, so that the sea surface elevation field can be viewed better. Purple star indicates where the epicenter is. Also annotated is Sendai, a city near the epicenter. Depth contours, valued at 200, 500, and from 1000 to 7000 with intervals of 1000 m, are also superimposed to indicate the topography.

sensed by the DART instrument through the motions of the seabed. The agreements for the secondary waves are not as good as for the primary ones, which we will come back to after comparisons for more stations. The other panels show the individual contributions by the initial $\boldsymbol{\eta}$, $\mathbf{U}$, and $\mathbf{V}$, respectively. The top-right panel and the bottom-left panel show that the contributions by the initial $\boldsymbol{\eta}$ and the initial $\mathbf{U}$ are on the same order, each accounting for about the half of the maximum observed amplitude. The initial $\mathbf{V}$ contributes little as shown in the bottom-right panel. This is because for the 2011 Tohoku tsunami, the initial velocities were mostly in the eastward direction. The equal contributions by the initial $\boldsymbol{\eta}$ and $\mathbf{U}$ suggest that we should not neglect the initial water mass transports in a tsunami source function. Such negligence has been common so far in tsunami modeling. Further discussions and explorations on this point alone should be interesting; however, this will require a separate paper.

The station DART 21418 is the closest to the source region among the DART buoys. Results for this station can provide us with confidence in our initial condition. We will now show the results for other stations to cover the near, mid-, and far fields. Figure 6 provides comparisons for the six such stations: DARTs 21413 and 21419 represent the near field, DARTs 51407 and 51425 the midfield, and DARTs 32411 and 32412 the far field. We show only the predictions with all three components of the source function. As we can see from the figure, the overall agreements between the model solutions and the DART buoy observations in all the fields are fairly good, indicating that both the GPS method and the ASGF method are working well together.

As we have noted above, the agreements for the secondary waves are not as good as for the primary ones. For station DART 21418 (Fig. 5), the amplitudes of the observed secondary waves are underpredicted, albeit the timing is still good. However, this does not seem to be a persistent pattern. In DARTs 21413 and 21416, we just see a reverse case. Generally speaking, the secondary waves are weaker signals and are more susceptible to imperfections of the initial condition, the neglected dynamics in the propagation model, the details in the local topography, the noises in the observations, etc. These secondary discrepancies might be reduced if our solutions were tsunami wave data assimilative. However, this is where we have also a point to emphasize: our solutions do not bear any feedback from the tsunami wave observations; our solutions are purely predictive in this sense, and can be made as soon as an earthquake triggers a tsunami rather than having to wait for tsunami waves to arrive at the observation sites. The overall good agreements between our predictions and the observations should be adequate for tsunami warnings. Having said that, we would like also to point out that our method can well support data assimilation, since Eq. (8) is already in the typical least squares form with which one can easily apply

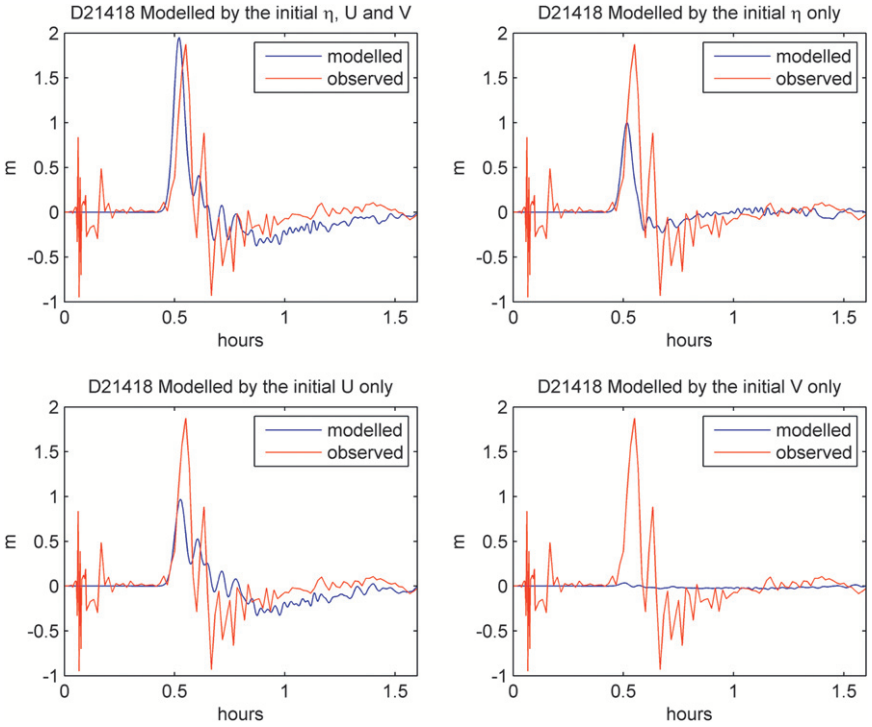

FIG. 5. Different versions of the prediction against the same observation at station DART 21418. (top left) Prediction modeled with the total initial condition including the initial sea level $\boldsymbol{\eta}$, and the initial mass transports **U** and **V**. Other three panels show the contributions by the initial $\boldsymbol{\eta}$, **U**, and **V** individually. Spikes in red at the beginning of the curves are the seismic rock waves.

various data fitting techniques to refine the initial condition as new tsunami wave data arrive.

5. Closing remarks

We have demonstrated the potential of combining our two recently proposed tsunami methods, the GPS method (Song 2007; Song et al. 2008) and the ASGF method (Xu 2007, 2011), into a system for fast tsunami predictions. Immediately following a coastal submarine earthquake, the GPS method can provide a tsunami source function constrained by motions of the coastal GPS stations sensed by satellites in real time. The precalculated ASGFs can then instantaneously transfer the source function to tsunami arrival time series at points of interest. We took the 2011 Tohoku tsunami as the validating case, and the comparisons of our predictions and DART observations were shown in Figs. 5 and 6. The overall good agreement between the predictions and the observations is encouraging. We do not mean to say that we are offering a ready-to-take solution for fast tsunami predictions. Rather, we view our exploration as a proof of concept. Theoretically, we think that the combination of the GPS and the ASGF methods is a way to go for fast tsunami predictions. Realistically, we know that there is still a lot of work to do to improve our approach, and our demonstration presented here is just a beginning.

Our tsunami source function is estimated from the GPS data for the seafloor motions, rather than the earthquake magnitude. It is the seafloor motions, not the earthquake magnitude, that are the direct source of a tsunami. The good agreement between the observed by the DART buoys and the predicted with the GPS-based source indicates that using the land-based GPS data is a promising way to go. However, the new way also comes with its own challenges. For example, in converting the 3D land displacement to initial sea level setup and water mass depth transports, the uncertainties include 1) the GPS data processing errors, particularly the vertical component; 2) the local bathymetric details and the exact fault locations; and 3) the empirical profile model used in deriving the seafloor motions from the GPS data [see Song (2007) and Song et al. (2008) for more details]. How to reduce these uncertainties certainly is a topic for further efforts. Another challenge lies in the coverage of coastal GPS station network. Evidently our GPS-based tsunami source inferring only applies to the regions where there is a land-based GPS network nearby. To establish an optimal GPS

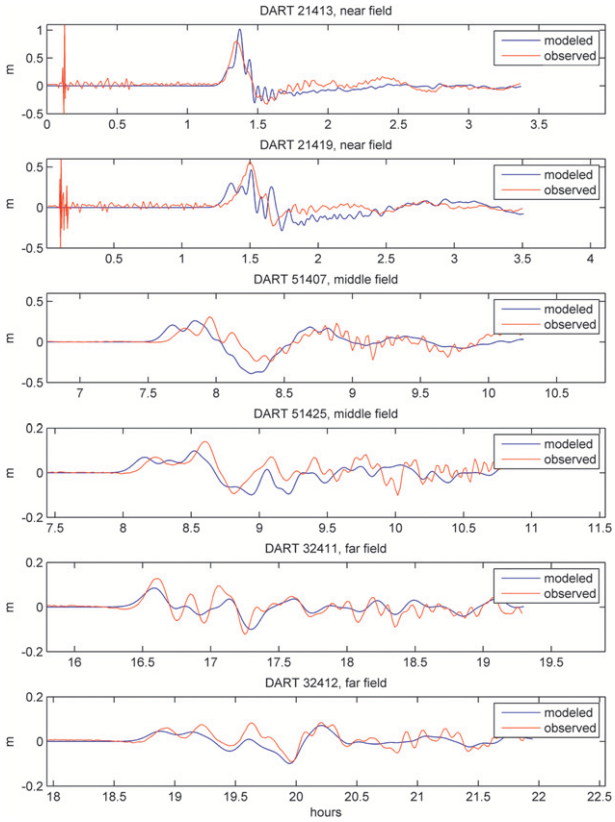

FIG. 6. Comparisons between the modeled and the observed for six stations from the near, mid-, and far fields.

station network to cover the coastal oceans worldwide is a topic for both research and international collaboration.

During our demonstration, we have also touched upon a few other points, such as the importance of the initial velocity components and using the data assimilation technique to improve the predictions. Each of these points itself is interesting but requires a separate paper. Also, to have an intercomparison study of our methods against others is not the goal here. Such an intercomparison study might be well necessary when one chooses a method for establishing a tsunami predicting system or for improving an existing one, but it is beyond the scope of this paper. We also wish our readers not to expect that our approach could also address the tsunami inundation problems—that would require a nonlinear and perhaps nonhydrostatic model. However, our approach does have a potential to quickly provide offshore boundary conditions to local inundation models.

Acknowledgments. We would like to express our gratitude to Dr. Allyn Clarke of the Bedford Institute of Oceanography, Department of Fisheries and Oceans Canada, for his careful review of the first edition of our manuscript and valuable suggestions. Our thanks also go to Ms. Shushan Song for her proofreading this edition of our manuscript. We would like also to gratefully acknowledge the support from our institutes for this work. The valuable comments from the anonymous reviewers are also greatly appreciated. Part of the research was carried out at the Jet Propulsion Laboratory, California Institute of Technology, under a contract with the National Aeronautics and Space Administration.

APPENDIX A

Algorithm for Calculating the All-Source Green's Functions

The MATLAB codes in Table A1 give an algorithm on how to calculate just the nth row of the power of the dynamics matrix without having to calculate the other rows: Each $\mathbf{r}$ during the iteration is one of the series $\mathbf{r}^{(k)}$, $(k = 0, 1, 2, \ldots)$, and is a row vector. The initial one, $\mathbf{r}^{(0)}$, is a row vector of the identity matrix; $\mathbf{r}^{(1)}$ is simply a copy of the nth row of the matrix $\mathbf{A}$, and $\mathbf{r}^{(2)}$ is the nth row of the second power of the matrix $\mathbf{A}$. The algorithm avoids the calculation of the whole second power of the matrix, $\mathbf{A}^2 = \mathbf{A} \times \mathbf{A}$; it only calculates the nth row of the power. The vector–matrix multiplication iterates to produce the higher power of the matrix for the needed row only. Since the identity matrix can be viewed as the 0th power of the matrix $\mathbf{A}$, and the matrix $\mathbf{A}$ can be viewed as the first power of itself, the series $\mathbf{r}^{(k)}$, $(k = 0, 1, 2, \ldots)$ can be uniformly viewed as the row of the kth power of the matrix $\mathbf{A}$.

If we denote $\mathbf{G}$ as a collector of the series $\mathbf{r}^{(k)}$ saved during the iteration—that is,

$$\mathbf{G} = [\mathbf{r}^{(0)}; \mathbf{r}^{(1)}; \ldots; \mathbf{r}^{(k_{\max})}], \tag{A1}$$

where the semicolons inside the bracket indicate the end of a previous row and the beginning of the next— then a simple matrix–vector multiplication of

$$\boldsymbol{\eta}_n(k) = \mathbf{G} \begin{bmatrix} \boldsymbol{\eta} \\ \mathbf{U} \\ \mathbf{V} \end{bmatrix}^{(0)} \tag{A2}$$

can then provide a solution time series at the POI in response to an initial setup anywhere in the model domain. The $\mathbf{G}$ matrix is the ASGF. In the above equation, $\boldsymbol{\eta}_n(k)$ represents the time series of the elevations at the nth η node. Note that the parenthesized k here is not in a superscript position. A parenthesized k in a normal position means a vector of time indexes, $k = (1, 2, \ldots, k_{\max})$.

For completeness, we present two additional tables, Table A2 and Table A3, for the algorithms that calculate

TABLE A1. MATLAB codes to calculate an ASGF.

Lines	Codes	Comments
1	**r** = zeros(1, *N*); **r**(*n*) = 1;	Initiate a delta-forcing row vector **r** at a single receiver point *n*
2	for $k = 1{:}k_{\max}$	Time looping to advance **r**
3	**r** = **r***__A__;	**r** is saved to disk at some regular time intervals
4	End	

TABLE A2. MATLAB codes to calculate an SSGF.

Lines	Codes	Comments
1	**c** = zeros(*N*, 1); **c**(*n*) = 1;	Initiate a delta-forcing column vector **c** at *n*
2	for $k = 1{:}k_{\max}$	Time looping to advance **c**
3	**c** = __A__*__c__;	**c** is saved to disk at a regular time interval
4	End	

the classical SSGF and its block–source version (BSGF). These two tables, together with the preceding one, put the three types of Green's functions on the same algorithmic footing, so that one can easily see what are common to them and where they differ. As we can see, the cost is the same for computing an SSGF or an ASGF; however, the former covers only one model grid point as the source point, whereas the latter covers all of the model grid points as potential source points. The former computes the responses at all of the model grid points, most of which will not be of interest, whereas the latter computes the responses only at the point that is of interest; the former has to repeat its computation for each additional source point and so does the latter for each additional point of interest (receiver). Points of interest are known but points of sources are not known prior to a real tsunami event; all of the model grid points can be potentially the source points, whereas points of interest are only a few, scattered along the coasts (and at some deep-water observation sites). The BSGF is just a ''blur'' version of the SSGF; it lumps many grid points into one big source point (a block source).

Finally, we would like to add a comment: the algorithms presented here for ASGFs, SSGFs, and BSGFs are all independent of the numerical details of the tsunami models from which these Green's functions are derived. This is to say that any tsunami model (supposedly linear), whose SSGFs (or rather the BSGFs) have been proved working well in ''predicting'' tsunamis because of its numerical merits achieved by many valuable refinements, can be easily switched to produce the ASGFs while all its numerical merits will still be inherited.

APPENDIX B

Formulas for the 2011 Tohoku-Oki Source Functions

The notation here is independent of the rest of the paper. Let (E, N, U) be the three-dimensional GPS or seismically derived seafloor displacements, which represent a motion of a grid size of Δx by Δy (a subfault) in this study. Based on the impulse–momentum principle of fluid mechanics (Vennard and Street 1982), the accelerated three-dimensional velocity of water particles in the vicinity of the moving seafloor can be written as

$$\Delta u_b(z) = \begin{cases} E/\tau & \text{if} \quad -h \le z \le -R_x = \min\{h, L_H|h_x|\} \\ 0 & \text{otherwise} \end{cases}, \tag{B1}$$

$$\Delta v_b(z) = \begin{cases} N/\tau & \text{if} \quad -h \le z \le -R_y = \min\{h, L_H|h_y|\} \\ 0 & \text{otherwise} \end{cases}, \tag{B2}$$

$$\Delta w_b(z) = (U + Eh_x + Nh_y)/\tau \quad -h \le z < 0, \tag{B3}$$

where Δ represents the impulse velocity only during the rise-time period τ of faulting; h is the ocean topography; and h_x and h_y are the eastward and northward slopes of the subfault surface, respectively. Also L_H is the effective scale of the horizontal motion, z is the vertical coordinate at the undisturbed ocean surface, and $\Delta u_b(z)$ and $\Delta v_b(z)$ are the bottom-water velocity within the range of R_x and R_y, respectively. Here, $\Delta w_b(z)$ is the vertical velocity because of the seafloor uplift. The velocity is actually the displacement divided by rise time τ (we have used 5–10 s for the 2004 Sumatra earthquake) within the water near the moving bottom. Notice that a flat bottom would have no contribution to the tsunami source because the slope is zero (i.e., $Rx = Ry = 0$). A parallel slip component would have no contribution either, because the slope in that direction is zero (i.e., $Rx = 0$ or $Ry = 0$).

It should be noted that the vertical acceleration of water particles does not contribute to the tsunami propagation, but the resultant sea surface perturbation does.

TABLE A3. MATLAB codes to calculate a BSGF.

Lines	Codes	Comments
1	**c** = zeros(*N*, 1); **c**(*v*) = 1;	Initiate a block–source *c* at a block of source points *v* where **v** is a vector of gridpoint indices
2	for $k = 1{:}k_{\max}$	Time looping to advance **c**
3	**c** = __A__*__c__;	**c** is saved to disk at a regular time interval
4	End	

Because the vertical velocity $\Delta w_b(z)$ can be approximated by the ocean bottom/sea surface perturbation with the relationship $dh(t)/dt \approx w_b(z)$, our vertical velocity condition of Eq. (B3) is actually equivalent to the conventional assumption of the initial sea surface perturbation (Tanioka and Satake 1996):

$$\eta_0(x, y, t) \approx \Delta h = U + Eh_x + Nh_y. \quad \text{(B4)}$$

This part is essentially the conventional tsunami source, from which the ocean would gain potential energy.

Now, we explain how the horizontal velocity can be applied to the ocean model. In the tsunami source, Eqs. (B1)–(B3), the only unknown parameter is the horizontal effective scale L_H. In the deep ocean, the linear-wave theory implies that the tsunami height is proportional to the total source energy: the potential energy due to the seafloor uplift and the kinetic energy due to the horizontal motions of water. Because the potential energy can be estimated from the seafloor uplift, the kinetic energy has to complement the total tsunami energy. It is found that $L_H = 1.5\ h_{\max}$ (the maximum of ocean depth) is a proper value for the 2004 Sumatra earthquake. This is what we have expected because L_H cannot be arbitrary and should be constrained by the ocean depth. The initial forcing (within the period $t < \tau$) for the horizontal momentum can be written as

$$u_0(x, y, z, t) = \Delta u_b(z), \quad \text{(B5)}$$

$$v_0(x, y, z, t) = \Delta v_b(z). \quad \text{(B6)}$$

It should be noted that the conditions apply to the ocean model only during the rise time and near the bottom of fault area. In summary, Eqs. (B4)–(B6) give the three-dimensional tsunami source, and all of them can be estimated in real time from the GPS-derived seafloor motions using the empirical profile method of Song (2007).

REFERENCES

Arakawa, A., and V. R. Lamb, 1977: Computational design of the basic dynamical process of the UCLA general circulation model. *Methods in Computational Physics,* J. Chang, Ed., Vol. 17, Academic Press, 173–265.

Ding, Y., Y. Jia, and S. S. Wang, 2004: Identification of Manning's roughness coefficients in shallow water flows. *J. Hydraul. Eng.,* **130,** 501–510, doi:10.1061/(ASCE)0733-9429(2004)130:6(501).

Fujii, Y., and K. Satake, 2007: Tsunami source of the 2004 Sumatra–Andaman earthquake inferred from tide gauge and satellite data. *Bull. Seismol. Soc. Amer.,* **97,** 5192–5207, doi:10.1785/0120050613.

——, and ——, 2008: Tsunami sources of the November 2006 and January 2007 great Kuril earthquakes. *Bull. Seismol. Soc. Amer.,* **98,** 1559–1571, doi:10.1785/0120070221.

——, ——, S. Sakai, M. Shinohara, and T. Kanazawa, 2011: Tsunami source of the 2011 off the Pacific coast of Tohoku earthquake. *Earth Planets Space,* **63,** 815–820.

Gica, E., M. Spillane, V. V. Titov, C. D. Chamberlin, and J. C. Newman, 2008: Development of the forecast propagation database for NOAA's Short-Term Inundation Forecast for Tsunamis (SIFT). NOAA Tech. Memo. OAR PMEL-139, 89 pp.

Johnson, J. M., and K. Satake, 1993: Source parameters of the 1957 Aleutian earthquake from tsunami waveforms. *Geophys. Res. Lett.,* **20,** 1487–1490.

——, ——, S. R. Holdahl, and J. Sauber, 1996: The 1964 Prince William Sound earthquake: Joint inversion of tsunami and geodetic data. *J. Geophys. Res.,* **101** (B1), 523–532.

Lauterjung, J., and the GITEWS Team, 2008: GITEWS—The German–Indonesian Tsunami Early-Warning System: Status and outlook. *Int. Disaster and Risk Conf.,* Davos, Switzerland, IDRC, 25 pp. [Available online at http://www.idrc.info/userfiles/image/presentations2008/Lauterjung_Joern_The_GermanIndonesian_Tsunami_Early_Warning_System_Status_and_Outlook.pdf.]

Moritz, H., 2000: Geodetic Reference System 1980. *J. Geod.,* **74,** 128–162, doi:10.1007/s001900050278.

NCTR, cited 2012a: DART (Deep-Ocean Assessment and Reporting of Tsunamis). [Available online at http://nctr.pmel.noaa.gov/Dart/index.html.]

——, cited 2012b: Forecast propagation database. [Available online at http://nctr.pmel.noaa.gov/propagation-database.html.]

——, cited 2012c: Japan (east coast of Honshu) tsunami, March 11, 2011. [Available online at http://nctr.pmel.noaa.gov/honshu20110311/.]

——, cited 2012d: Tsunami forecasting. [Available online at http://nctr.pmel.noaa.gov/tsunami-forecast.html.]

——, cited 2012e: Unit sources by region. [Available online at http://nctr.pmel.noaa.gov/unit_sources.html.]

Okada, Y., 1985: Surface deformation due to shear and tensile faults in a half-space. *Bull. Seismol. Soc. Amer.,* **75,** 1135–1154.

Romano F., A. Piatanesi, S. Lorito, N. D'Agostino, K. Hirata, S. Atzori, Y. Yamazaki, and M. Cocco, 2012: Clues from joint inversion of tsunami and geodetic data of the 2011 Tohoku-Oki earthquake. *Sci. Rep.,* **2,** 385, doi:10.1038/srep00385.

Satake, K., 1985: The mechanims of the 1983 Japan Sea earthquake as inferred from long-period surface waves and tsunamis. *Phys. Earth Planet. Inter.,* **37,** 249–260.

——, 1987: Inversion of tsunami waveforms for the estimation of a fault heterogeneity: Method and numerical experiments. *J. Phys. Earth,* **35,** 241–254.

——, 1989: Inversion of tsunami waveforms for the estimation of heterogeneous fault motion of large submarine earthquakes: The 1968 Tokachi-Oki and 1983 Japan Sea earthquakes. *J. Geophys. Res.,* **94** (B5), 5627–5636.

Shuto, N., 1991: Numerical simulation of tsunamis—Its present and near future. *Nat. Hazards,* **4,** 171–191.

Sommerfeld, A., 1949: *Partial Differential Equations in Physics.* Pure and Applied Mathematics Series, Vol. 1, Academic Press, 335 pp.

Song, Y. T., 2007: Detecting tsunami genesis and scales directly from coastal GPS stations. *Geophys. Res. Lett.,* **34,** L19602, doi:10.1029/2007GL031681.

——, and S.-C. Han, 2011: Satellite observations defying the long-held tsunami genesis theory. *Remote Sensing of the Changing Oceans,* D. Tang, Ed., Springer-Verlag, 327–342.

——, C. Ji, L.-L. Fu, V. Zlotnicki, C. K. Shum, Y. Yi, and V. Hjorleifsdottir, 2005: The 26 December 2004 tsunami

source estimated from satellite radar altimetry and seismic waves. *Geophys. Res. Lett.,* **23,** L20601, doi:10.1029/2005GL023683.

——, L.-L. Fu, V. Zlotnicki, C. Ji, V. Hjorleifsdottir, C. K. Shum, and Y. Yi, 2008: The role of horizontal impulses of the faulting continental slope in generating the 26 December 2004 tsunami. *Ocean Modell.,* **20,** 362–379, doi:10.1016/j.ocemod.2007.10.007.

——, I. Fukumori, C. K. Shum, and Y. Yi, 2012: Merging tsunamis of the 2011 Tohoku-Oki earthquake detected over the open ocean. *Geophys. Res. Lett.,* **39,** L05606, doi:10.1029/2011GL050767.

Tan, W., 1992: *Shallow Water Hydrodynamics: Mathematical Theory and Numerical Solution for a Two-Dimensional System of Shallow Water Equations.* Oceanography Series, Vol. 55, Elsevier, 434 pp.

Tanioka, Y., and K. Satake, 1996: Tsunami generation by horizontal displacement of ocean bottom. *Geophys. Res. Lett.,* **23,** 861–864.

Titov, V. V., and F. I. González, 1997: Implementation and testing of the Method of Splitting Tsunami (MOST) model. NOAA Tech. Memo. ERL PMEL-112 (PB98-122773), NOAA/Pacific Marine Environmental Laboratory, 11 pp.

——, ——, E. N. Bernard, M. C. Eble, H. O. Mofjeld, J. C. Newman, and A. J. Venturato, 2005: Real-time tsunami forecasting: Challenges and solutions. *Nat. Hazards,* **35,** 41–58.

Vennard, J. K., and R. L. Street, 1982: *Elementary Fluid Mechanics.* 6th ed. John Wiley & Sons, 689 pp.

Weinstein, S., and P. Lundgren, 2008: Finite fault modeling in a tsunami warning center context. *Pure Appl. Geophys.,* **165,** 451–474.

Xu, Z., 2007: The all-source Green's function and its applications to tsunami problems. *Sci. Tsunami Hazards,* **26,** 59–69.

——, 2011: The all-source Green's function of linear shallow water dynamic system: Its numerical constructions and applications to tsunami problems. *The Tsunami Threat—Research and Technology,* Nils-Axel Mörner, Ed., Intech, 509–540. [Available online at http://www.intechopen.com/books/the-tsunami-threat-research-and-technology/.]